RSC Advances

PAPER

View Article Online
View Journal | View Issue

Cite this: *RSC Adv.*, 2021, **11**, 19908

Electron beam lithography for direct patterning of MoS_2 on PDMS substrates†

Gil Jumbert,[ab] Marcel Placidi,[cd] Francesc Alzina,[a] Clivia M. Sotomayor Torres[ae] and Marianna Sledzinska *[a]

Precise patterning of 2D materials into micro- and nanostructures presents a considerable challenge and many efforts are dedicated to the development of processes alternative to the standard lithography. In this work we show a fabrication technique based on direct electron beam lithography (EBL) on MoS_2 on polydimethylsiloxane (PDMS) substrates. This easy and fast method takes advantage of the interaction of the electron beam with the PDMS, which at high enough doses leads to cross-linking and shrinking of the polymer. At the same time, the adhesion of MoS_2 to PDMS is enhanced in the exposed regions. The EBL acceleration voltages and doses are optimized in order to fabricate well-defined microstructures, which can be subsequently transferred to either a flexible or a rigid substrate, to obtain the negative of the exposed image. The reported procedure greatly simplifies the fabrication process and reduces the number of steps compared to standard lithography and etching. As no additional polymer, such as polymethyl methacrylate (PMMA) or photoresists, are used during the whole process the resulting samples are free of residues.

Received 2nd February 2021
Accepted 24th May 2021

DOI: 10.1039/d1ra00885d

rsc.li/rsc-advances

Introduction

2D materials, such as transition metal dichalcogenides (TMDs), offer unprecedented possibilities in applications such as electronics, optics or sensing.[1,2] However, the precise control of the size and shape of 2D materials is critical for the fabrication of functional devices. As for now, their integration in electronic circuits requires a large number of fabrication steps, such as lithography, etching, and transfer.[3] In the future the number of these steps will increase with the increasing complexity of the devices. At the same time 2D materials are particularly sensitive to contamination and residues, which can introduce defects, doping and seriously degrade their optical and electronic properties.[4–7] Moreover, many cleaning techniques commonly used in silicon industry, such as strong acids or oxygen plasma, can no longer be used for 2D materials processing.

Therefore, many efforts have been dedicated to the development of cleaner alternative fabrication methods. Instead of the electron beam or optical lithography[8,9] one of the ideas has been to directly pattern the substrate and achieve the selective growth in the desired areas.[10,11] In the case of MoS_2 on SiO_2/Si substrates, photolithography, O_2 plasma and a specific chemical surface treatment was applied before chemical vapour deposition (CVD) growth.[12] This process resulted in a single layer MoS_2 with desired shapes and a minimal feature lateral size of 2 μm. Similarly chalcogenide crystals of Bi_2Se_3 and In_2Se_3 were grown by a method which combines solvent nanoimprinting with van der Waals epitaxy on mica substrates.[13]

Other alternative nanofabrication approaches have been developed to directly pattern the 2D materials on different substrates. In order to avoid the use of a photoresist or PMMA it has been proposed to pattern graphene films through a stencil mask by magnetic-assisted ultraviolet ozone treatment.[14] However, high resolution patterns would be difficult to achieve using such a method. Furthermore, laser ablation has been reported as a relatively fast and precise method in order to thin a multilayer MoS_2 down to a monolayer,[15] bilayer and trilayer[16] with both vertical and lateral control and maintaining good electronic properties. Similarly an optothermoplasmonic nanolithography is possible for 2D films placed on top of substrates made of gold nanoparticles.[17] It takes advantage of the localized surface plasmon resonances, which enhance thermal oxidation and sublimation of the films when the substrate is exposed to the laser irradiation. However, the main drawback of this method is the need of a metallic substrate.

In this work, we report an easy patterning method for MoS_2 on PDMS, which is the most common material employed for 2D

[a]*Catalan Institute of Nanoscience and Nanotechnology (ICN2), CSIC, BIST, Campus UAB, Bellaterra, 08193 Barcelona, Spain. E-mail: marianna.sledzinska@icn2.cat*
[b]*Departament de Fisica, Universitat Autònoma de Barcelona, Bellaterra, E-08193 Barcelona, Spain*
[c]*Catalonia Institute for Energy Research (IREC), Jardins de les Dones de Negre 1, Sant Adrià de Besòs, Spain*
[d]*Photovoltaic Group, Electronic Engineering Department, Polytechnic University of Catalonia (UPC), Barcelona, Spain*
[e]*ICREA, Pg. Lluís Companys 23, 08010 Barcelona, Spain*

† Electronic supplementary information (ESI) available. See DOI: 10.1039/d1ra00885d

materials exfoliation and transfer. The process is based on direct electron beam lithography (EBL), however, instead of using a standard PMMA mask and dry etching pattern transfer, we take advantage of the interaction between the electron beam and the MoS_2 on the PDMS. The electron beam exposure strongly enhances the adhesion of MoS_2 to the PDMS and afterwards the film can be dry-transferred either to a rigid substrate, such as Si/SiO_2, or to another flexible substrate, such as PET, in order to obtain the negative of the exposed image. The main advantage of this method is the significant reduction of the number of fabrication steps to three (transfer to PDMS, EBL and transfer to the final substrate). The use of EBL allows for exposition of arbitrary patterns without a physical mask and with the resolution comparable to the above-discussed processes.

Nanofabrication process

MoS_2 was grown on glass substrates, by direct sulfurization of a Mo thin film layer. It is a kinetic synthesis method, which has also been used to produce structures such as nanotubes or fullerene-like nanoparticles.[18,19] In this way, both horizontally and vertically aligned layers can be formed, depending on the sample thickness and process conditions.[20–22] In this work a continuous MoS_2 polycrystalline film with thickness of 2 nm is used. Detailed sample characterisation can be found in the ESI (ESI, Fig. S1 to S4†).

Polymer-free, wet transfer was performed in order to transfer the MoS_2 from the original glass substrate to PDMS films (GelPak).[21] The direct transfer procedure consisted in bringing the PDMS film into contact with MoS_2 surface. A drop of DI water was placed with a pipette at the interface of the PDMS and the MoS_2/glass. Due to the surface tension difference, the MoS_2 layer is lifted off from the glass substrate. The PDMS is then peeled off together with the attached MoS_2 during approx. 5–10 s (ESI, Fig. S5†). The process was performed in the ambient environment (20 °C, 40% relative humidity).

The EBL was performed to directly pattern the MoS_2 on PDMS samples (Fig. 1(a)). Parameters such as the exposition dose and acceleration voltage are discussed in the section below.

Finally, after the exposure the MoS_2 film was dry-transferred to the final substrate, where we obtained the negative of the exposed pattern (Fig. 1(b)). For the dry transfer process, the patterned PDMS was brought in contact with the final substrate (Si/SiO_2 or PET). A finger-pressure was applied for a few minutes. Then the PDMS was gently peeled off during approx. 5–10 s. In general, we found that the transfer process quality does not strongly depend on the pressure and time. The process was performed in the ambient environment (20 °C, 40% relative humidity).

Results and discussion

While PDMS has been extensively used in nanoimprint lithography not many works have been dedicated to its use in EBL and, more specifically, to its interaction with an electron beam. Such a study can give rise to a new nanofabrication tool for 2D materials patterning. It has been reported that during *e*-beam exposure methyl groups of the PDMS are removed allowing the backbones of different polymer chains to become cross-linked (Fig. 2(a)). However, at large doses, the electrons also can cause chain scission and the formation of other chemical species.[23,24] At the same time, the PDMS hardness increases with the increase in the exposure dose, which has been attributed to the increase in cross-link density and decrease in molecular mobility. Higher degree of cross-linking results in a tighter network, which is responsible for the increase *e* in hardness.[25] Moreover, a monotonic increase in the Young's modulus of PDMS from ~50 to ~350 MPa as a function of the *e*-beam dose was reported.[26]

In a previous work, we studied the interactions at the interface between MoS_2 and PDMS induced by an *e*-beam[27] unveiling that well-defined micro-patterns can be obtained in the MoS_2 regions. Due to the insulating nature of the PDMS the majority of the dose is accumulated on the surface and the MoS_2 film-PDMS interface undergoes strong cross-linking. We have observed stronger adhesion of the MoS_2 to the PDMS substrate, enhanced by the short-bonded PDMS chains.

First of all, a set of 200 μm long rectangles with nominal width of1 μm have been exposed at three acceleration voltages of 10, 20 and 30 kV and currents of 0.12, 0.14 and 0.15 nA, respectively. In Fig. 2(b) we compare the real width of a rectangle designed to be of 1 μm exposed at two doses, 100 and 700 μC cm^{-2}, for each of the acceleration voltages. Higher acceleration voltages and smaller doses yield thinner patterns.

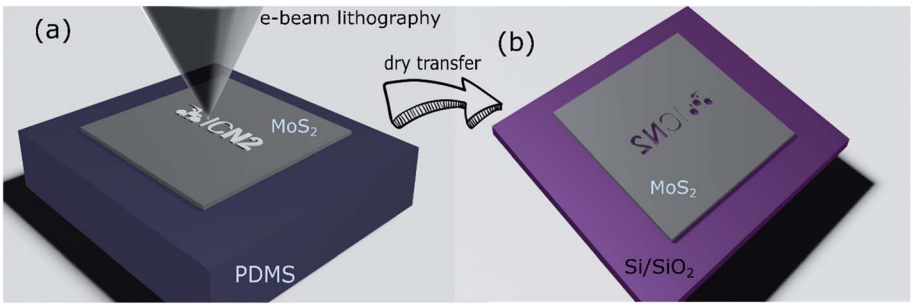

Fig. 1 Schematic representation of the fabrication process. (a) Electron beam lithography on MoS_2 on PDMS substrate followed by dry transfer to (b) the final substrate where the negative of the exposed pattern is obtained.

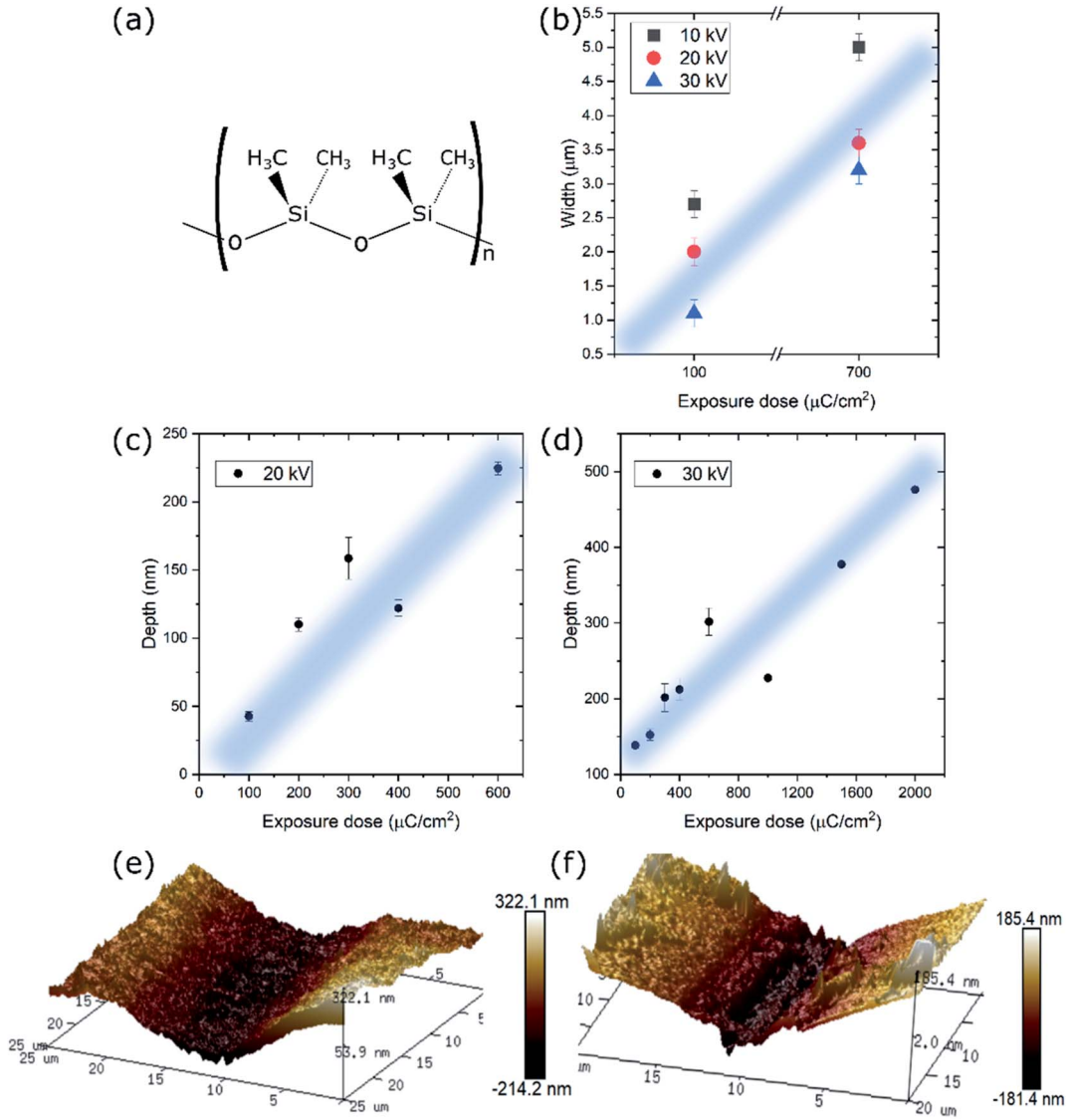

Fig. 2 (a) Schematic of a section of PDMS polymer chain. (b) Real width of the (nominal) 1 μm wide rectangle exposed at 10, 20 and 30 kV and varying doses. Depth of the of the exposed features in MoS_2/PDMS as a function of exposure dose for (c) 20 kV and (d) 30 kV acceleration voltage. 3D representations of the AFM images of rectangles exposed at (e) 20 kV and 600 μC cm^{-2} dose (f) 30 kV and 300 μC cm^{-2} dose.

Clearly, the closest to the original design is the rectangle exposed at 30 kV and the dose of 100 μC cm^{-2} (1.1 ± 0.2 μm). Therefore, we can conclude that the easily achievable minimum size of the features exposed on the MoS_2/PDMS is between 1 and 2 μm, comparable to the techniques reported previously.

Secondly, a set of 1 mm long rectangles with nominal widths between 1 and 25 μm have been exposed at the same three acceleration voltages. At the voltages of 20 and 30 kV the exposed patterns were clearly visible under the optical microscope because of the strong cross-linking of the PDMS. We performed AFM on the set of rectangles exposed with doses from 100 to 2000 μC cm^{-2} in order to determine the level of contraction of the PDMS due to the *e*-beam interaction. The results are compared in Fig. 2(c) and (d). For both voltages we observe a linear increase in depth of the features with the increasing dose. As expected, higher acceleration voltages lead to deeper penetration of the electrons in the PDMS which in consequence leads to larger depth of exposed features. Examples of the AFM profiles are shown in Fig. 2(e) and (f). Patterns exposed using 10 kV acceleration voltage yield small contrast under the optical microscope, therefore it was not possible to locate them for the AFM measurements (Fig. S6†). However, after the dry transfer to Si/SiO_2 the negatives of the patterns were clearly visible under the optical microscope. This further confirms that the penetration depth and the resulting PDMS contraction are acceleration dependent. In this work we have opted for exposition using 20 kV acceleration voltage, which combines good visibility under optical microscope and smaller contraction of the PDMS and, accordingly, shallow and narrow patterns.

All exposure doses between 100 and 1000 μC cm^{-2} generate well defined rectangles, as seen in the optical microscope

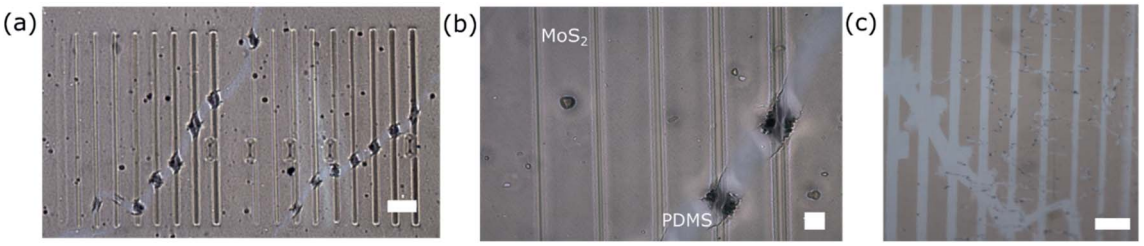

Fig. 3 (a) Optical image of the set of 1 mm long lines with varying widths exposed at 20 kV. Scale bar 100 μm. (b) Detail of the sample. The well-defined lines are only visible where the MoS_2 film is present. Scale bar 30 μm. (c) The sample transferred to PET substrate. Scale bar 100 μm.

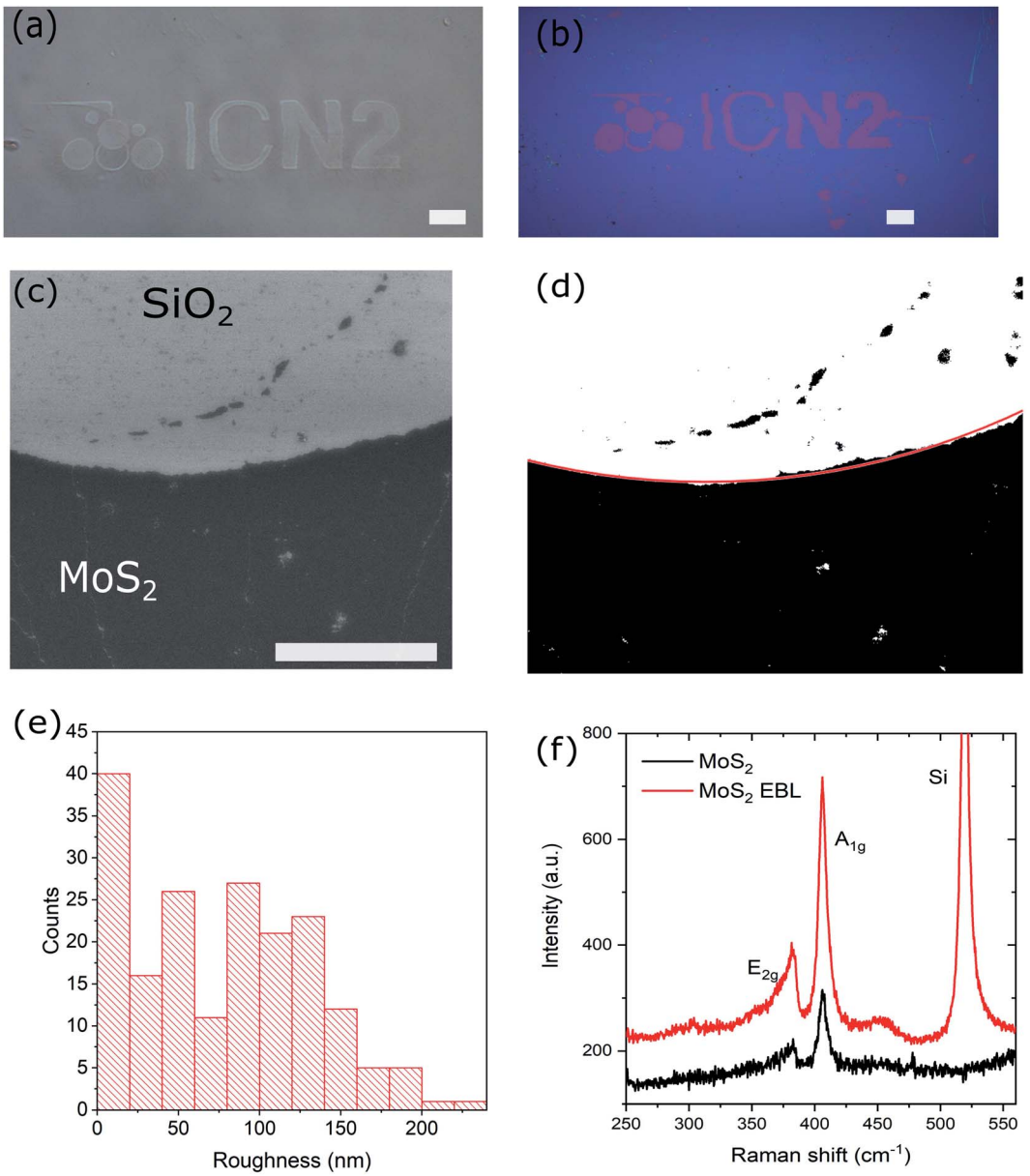

Fig. 4 (a) Example of an optical image of MoS_2 layer on PDMS after EBL, exposed at 20 kV and 300 μC cm^{-2} dose. (b) Optical image of MoS_2 layer after EBL transferred to Si/SiO_2 substrate. Scale bars 20 μm. (c) SEM image of the detail of the transferred pattern. Scale bar 5 μm. (d) Processed image of (c). Red curve indicates the segmentation of the pattern. (e) Distribution of roughness calculated from the segmented pattern. (f) Raman spectra of the MoS_2 layer on original growth substrate and transferred to Si/SiO_2 after EBL.

(Fig. 3(a) and (b)). The MoS_2 can be transferred to the PET film using dry transfer in order to obtain a well-defined negative of the exposed patterns (Fig. 3(c) and S7†). The thinnest lines which can be successfully transferred are of about 2 μm at the exposure dose of 100 μC cm^{-2}.

However, the patterns are only well exposed in the regions where MoS_2 is present on the PDMS. In the regions where the MoS_2 is not present (Fig. 3(b) and S8†) we observe that PDMS colour changed to almost black and the pattern is not well defined. We believe this is due to the fact that MoS_2 is conductive and helps eliminate extra charge, in a similar way in which a conductive polymer or thin metal layer is used for EBL on insulating substrates.

To assess the potential of the present method, we patterned and transferred a more complex design than the simple rectangles, *i.e.*, the ICN2 logo. The design was exposed with EBL using 20 kV and various doses between 100 and 1000 μC cm^{-2}. Optical images of the exposed sample and the transferred MoS_2 pattern to Si/SiO_2 are shown in Fig. 4(a) and (b), respectively. All of the exposure doses led to a good pattern definition and a successful transfer. A SEM image of a detail of the fabricated sample is shown in Fig. 4(c).

Using Matlab the SEM image was converted to black and white (Fig. 4(d)). In the resulting image, the pixels corresponding to MoS_2 pattern were black while the pixels of the background were white. The MoS_2 pattern was segmented by an arch of a circle fitted on the boundary by an iterative process. In the process the white area inside the arch and black area outside were maximized. Fig. 4(e) represents the roughness distribution, calculated as the distances between the pattern edge and the fitted arch. From the latter, we can extract an average (root mean square) roughness of the transferred patterns of about 100 nm, which proves that our technique is suitable for fabricating microstructures.

Raman spectra taken on both as-grown and transferred layers show no structural changes occurred in the material during the processing (Fig. 4(f)). Since no carrier polymer is used during the entire process the presence of organic contamination or residues is minimized. However, in some of the samples we have observed wrinkles and fractures of the MoS_2 film after the transfer from PDMS to the Si/SiO_2 (Fig. S9†). This effect is not caused directly by the EBL, but by the fact that large area transfer of ultrathin 2D materials is difficult to optimize. The fractures can occur both during the wet transfer to PDMS as well as during the dry transfer to the final substrate. Also polycrystalline MoS_2 has a relatively low fracture strength, in order of 5%, making it prone to breaking.[27] However, we believe it should be possible to perform the same process on the CVD grown single crystalline MoS_2 or exfoliated flakes, which will have more possibilities for a successful transfer and device applications. The crystalline MoS_2 has much higher Young modulus and its critical strain increases significantly when placed on an underlying substrate.[28,29]

One possible application of the proposed process could be in the field of micro- and nanoelectronics. 2D materials offer higher mobility than that of silicon and better scalability, which can lead to producing ultra-low noise field effect transistors and radiofrequency components with low cross talk and radiative losses and thus improved performance. Properly fabricated 2D transistor arrays are crucial for scale-up applications.[30,31]

Another application which can potentially benefit from our fabrication technique is the hydrogen evolution reaction (HER). MoS_2 has become one of the most promising electrocatalysts for both the HER as well as for hydro-desulfurization (HDS) of sulfur-rich hydrocarbon fuels.[32,33] Specifically, the edges of MoS_2 nanostructures are known to be far more active as compared to its basal planes. Bulk MoS_2 has relatively low electrical conductivity and small number of catalytically active edges, which seriously compromises its HER and HDS catalytic performance. On the other hand, patterning of MoS_2 thin films increases the number of active edges as well as allows for spatial tuning of the edge density for local catalytic reactions. The possibility for transfer to arbitrary substrates can further increase the process efficiency.

Conclusions

In this work we have studied the interaction between an electron beam and the PDMS/MoS_2 interface. We observed that exposure to the *e*-beam leads to cross-linking and contraction of PDMS, where the feature depth depends on the acceleration voltage and is roughly linearly proportional to the exposure dose. This effect was used to develop a new fabrication technique based on direct EBL on MoS_2 on PDMS substrates. This easy and fast method allows fabricating well-defined microstructures, which can be subsequently transferred to either a rigid or flexible substrate, to obtain a negative of the exposed image. As no additional polymer, such as PMMA, is used during the EBL the resulting samples are free of residues. While this technique has been proven on MoS_2 we believe it can be used for a variety of conducting and semiconducting 2D materials, as the mechanism behind the technique relies on the interaction between the electron beam and the PDMS.

Experimental methods

MoS_2 characterisation

Atomic force microscope topographical images were obtained using a Nanoscope IV controller and a Dimension 3100 head (Veeco). SEM images were taken in the FEI Quanta 650FEG ESEM and the FEI MAGELLAN 400L. Raman scattering measurements were performed using the Horiba T64000 Raman spectrometer and a 532 nm laser (cobolt). The Raman spectra at each point was obtained at the same incident laser power (0.3 mW) and integrated for the same amount of time (180 s). Elphy Quantum (Inspect F50 FEI SEM based system) was used for EBL. High-resolution imaging of the structure and morphology of the samples was obtained using the FEI Tecnai F20 in TEM and scanning TEM (STEM) modes.

Conflicts of interest

There are no conflicts of interest to declare.

Acknowledgements

ICN2 is funded by the CERCA program/Generalitat de Catalunya, and is supported by the Severo Ochoa program from Spanish MINECO (Grant No. SEV-2017-0706). We acknowledge support from EU Project NANOPOLY (GA 289061) and the Spanish MICINN project SIP (PGC2018-101743-B-I00). MP acknowledges the financial support from Spanish MICINN within the Ramón y Cajal Program (RYC-2017-23758).

References

1 D. Jariwala, V. K. Sangwan, L. J. Lauhon, T. J. Marks and M. C. Hersam, *ACS Nano*, 2014, **8**, 1102.
2 W. Choi, N. Choudhary, G. H. Han, J. Park, D. Akinwande and Y. H. Lee, *Mater. Today*, 2017, **20**, 116.
3 Y. Chen, X.-L. Gong and J.-G. Gai, *Adv. Sci.*, 2016, **3**, 1500343.
4 T. Hallam, N. C. Berner, C. Yim and G. S. Duesberg, *Adv. Mater. Interfaces*, 2014, **1**, 1400115.
5 L. Gammelgaard, J. M. Caridad, A. Cagliani, D. M. A. Mackenzie, D. H. Petersen, T. J. Booth and P. Bøggild, *2D Mater*, 2014, **1**, 035005.
6 W. Choi, M. A. Shehzad, S. Park and Y. Seo, *RSC Adv.*, 2017, **7**, 6943.
7 A. Quellmalz, X. Wang, S. Sawallich, B. Uzlu, M. Otto, S. Wagner, Z. Wang, M. Prechtl, O. Hartwig, S. Luo, G. S. Duesberg, M. C. Lemme, K. B. Gylfason, N. Roxhed, G. Stemme and F. Niklaus, *Nat. Commun.*, 2021, **12**, 917.
8 L. Ju, B. Geng, J. Horng, C. Girit, M. Martin, Z. Hao, H. A. Bechtel, X. Liang, A. Zettl, Y. R. Shen and F. Wang, *Nat. Nanotechnol.*, 2011, **6**, 630.
9 Y. Chen, N. Zhang, Y.-F. Li, Y.-G. Bi, Y.-Y. Yue, J. Feng and H.-B. Sun, *Adv. Opt. Mater.*, 2018, **6**, 1701348.
10 K. S. Kim, Y. Zhao, H. Jang, S. Y. Lee, J. M. Kim, K. S. Kim, J.-H. Ahn, P. Kim, J.-Y. Choi and B. H. Hong, *Nature*, 2009, **457**, 706.
11 Z. Liu, L. Ma, G. Shi, W. Zhou, Y. Gong, S. Lei, X. Yang, J. Zhang, J. Yu, K. P. Hackenberg, A. Babakhani, J.-C. Idrobo, R. Vajtai, J. Lou and P. M. Ajayan, *Nat. Nanotechnol.*, 2013, **8**, 119.
12 Y. Guo, P.-C. Shen, C. Su, A.-Y. Lu, M. Hempel, Y. Han, Q. Ji, Y. Lin, E. Shi, E. McVay, L. Dou, D. A. Muller, T. Palacios, J. Li, X. Ling and J. Kong, *Proc. Natl. Acad. Sci. U. S. A.*, 2019, **116**, 3437.
13 W. Zheng, T. Xie, Y. Zhou, Y. L. Chen, W. Jiang, S. Zhao, J. Wu, Y. Jing, Y. Wu, G. Chen, Y. Guo, J. Yin, S. Huang, H. Q. Xu, Z. Liu and H. Peng, *Nat. Commun.*, 2015, **6**, 6972.
14 Y. Wu, H. Tao, S. Su, H. Yue, H. Li, Z. Zhang, Z. Ni and X. Chen, *Sci. Rep.*, 2017, **7**, 1.
15 A. Castellanos-Gomez, M. Barkelid, A. M. Goossens, V. E. Calado, H. S. J. van der Zant and G. A. Steele, *Nano Lett.*, 2012, **12**, 3187.
16 L. Hu, X. Shan, Y. Wu, J. Zhao and X. Lu, *Sci. Rep.*, 2017, **7**, 15538.
17 L. Lin, J. Li, W. Li, M. N. Yogeesh, J. Shi, X. Peng, Y. Liu, B. B. Rajeeva, M. F. Becker, Y. Liu, D. Akinwande and Y. Zheng, *Adv. Funct. Mater.*, 2018, **28**, 1803990.
18 R. Tenne, L. Margulis, M. Genut and G. Hodes, *Nature*, 1992, **360**, 444.
19 Y. Feldman, E. Wasserman, D. J. Srolovitz and R. Tenne, *Science*, 1995, **267**, 222.
20 D. Kong, H. Wang, J. J. Cha, M. Pasta, K. J. Koski, J. Yao and Y. Cui, *Nano Lett.*, 2013, **13**, 1341.
21 M. Sledzinska, B. Graczykowski, M. Placidi, D. S. Reig, A. E. Sachat, J. S. Reparaz, F. Alzina, B. Mortazavi, R. Quey, L. Colombo, S. Roche and C. M. S. Torres, *2D Mater*, 2016, **3**, 035016.
22 M. Sledzinska, R. Quey, B. Mortazavi, B. Graczykowski, M. Placidi, D. Saleta Reig, D. Navarro-Urrios, F. Alzina, L. Colombo, S. Roche and C. M. Sotomayor Torres, *ACS Appl. Mater. Interfaces*, 2017, **9**, 37905.
23 J. Bowen, D. Cheneler and A. P. G. Robinson, *Microelectron. Eng.*, 2012, **97**, 34.
24 M. T. Russell, L. S. C. Pingree, M. C. Hersam and T. J. Marks, *Langmuir*, 2006, **22**, 6712.
25 R. Giri, M. S. Sureshkumar, K. Naskar, Y. K. Bharadwaj, K. S. S. Sarma, S. Sabharwal and G. B. Nando, *Adv. Polym. Technol.*, 2009, **27**, 98.
26 M. J. P. Biggs, M. Fernandez, D. Thomas, R. Cooper, M. Palma, J. Liao, T. Fazio, C. Dahlberg, H. Wheadon, A. Pallipurath, A. Pandit, J. Kysar and S. J. Wind, *Adv. Mater.*, 2017, **29**, 1702119.
27 M. Sledzinska, G. Jumbert, M. Placidi, A. Arrighi, P. Xiao, F. Alzina and C. M. Sotomayor Torres, *ACS Appl. Electron. Mater.*, 2020, **2**, 1169.
28 Y. Li, P. Chen, H. Liu, J. Peng, F. Gao and N. Luo, *Phys. Chem. Chem. Phys.*, 2019, **21**, 19115.
29 Y. Li, P. Chen, H. Liu, J. Peng and N. Luo, *J. Appl. Phys.*, 2021, **129**, 014302.
30 H. Nam, S. Wi, H. Rokni, M. Chen, G. Priessnitz, W. Lu and X. Liang, *ACS Nano*, 2013, **7**, 5870.
31 M. G. Stanford, P. D. Rack and D. Jariwala, *npj 2D Mater. Appl.*, 2018, **2**, 1.
32 A. Parija, Y.-H. Choi, Z. Liu, J. L. Andrews, L. R. De Jesus, S. C. Fakra, M. Al-Hashimi, J. D. Batteas, D. Prendergast and S. Banerjee, *ACS Cent. Sci.*, 2018, **4**, 493.
33 X. Kong, X. Shen, C. Zhang, S. Norooz Oliaee and Z. Peng, *Inorg. Chem. Front.*, 2016, **3**, 1376.